24th INTERNATIONAL CONGRESS ON SOUND AND VIBRATION
23–27 July 2017, London

A COMPRESSIBLE IMMERSED BOUNDARY METHOD FOR THE FLOW-INDUCED NOISE SIMULATION

Long Cheng, Lin Du, Xiaodong Jing and Xiaofeng Sun

Fluid and Acoustic Engineering Laboratory (FAEL), School of Energy and Power Engineering, Beihang University, Beijing 100191, P. R. CHINA
email: Long.Cheng@buaa.edu.cn

Guotun Hu

China Academy of Launch Vehicle Technology, Beijing 100076, P.R.CHINA

A numerical body force model of immersed boundary method is derived in this paper, to simulate the flow-induced noise from complex geometries by solving the compressible Navier-Stokes equations on a fixed Cartesian grid. To obtain the numerical form of the body force, a relevance matrix named "influence matrix" is constructed to accurately satisfy the no-slip wall boundary conditions via the Dirac delta function. The singularity of the Dirac delta function is eliminated by involving a smoothed approximation, both the low-storage Cholesky decomposition and preconditioned conjugate gradient methods for the highly sparse influence matrix are developed to solve the linear equations. The high-order finite difference schemes and nonlinear nonreflecting boundary conditions are employed. In order to validate the computational model, laminar flow around a circular cylinder is simulated. Both the flow and sound fields are compared with the previous results. Furthermore, the radiated sound fields from an oscillating circular cylinder in a uniform flow are studied. The relationship between the oscillating frequency and the radiated sound is presented. All these numerical studies exhibit the capacity of the proposed immersed boundary method to deal with the stationary or even moving wall boundary conditions in the computational aeroacoustics.
Keywords: body force model, flow-induced noise, oscillating circular cylinder.

1. Introduction

Prediction for the flow-induced noise from moving solid boundary is a challenging but important issue in the low-level noise design of modern aircraft. In order to get a profound comprehension for the physical processes of sound generation and propagation, numerical methods, especially the computational aeroacoustics (CAA), have been widely used in the past. When combined with the direct noise computation or acoustic analogy method, CAA has been identified as a powerful tool in the noise predictions such as the jet noise [1] and the slat noise [2] in high lift devices.

However, it's usually difficult for CAA to deal with moving-boundary problems [3][4], such as fan noise, rotorcraft noise or vortex-induced vibration/noise. Due to the low dissipation and low dispersion requirements of the numerical schemes for CAA, two puzzles usually exist: the mostly used moving-grid technique in computational fluid dynamics (CFD), however, is difficult to be adopted in CAA due to the high demand for the computational grid; the real-time high-resolution interpolation is so complicated and time-consuming if the overset grid is used. Actually, the moving-boundary problem in CAA also refers to the fluid-structure interaction (FSI) problem [5], which is one of the classical problems in CFD community. Besides the moving-grid and overset grid techniques in CFD community, the immersed boundary (IB) method is a promising method for FSI

problems and has been widely identified in incompressible [6] flows. Recently, Seo and Mittal [7] has developed a ghost-cell IB method to simulate the acoustic scattering and flow-induced noise problems. In 2012, Sun et al. [8][9] developed a relevance matrix technique of IB method named "influence matrix method(IMM)" to accurately calculate the body force, which can be used to replace the hard or soft wall boundary conditions. IMM allows a big Courant-Friedrich-Lax (CFL) number due to the combination of the continuous and the discretized forcing methods.

In this paper, a more general form of the IMM is derived to simulate the no-slip wall boundary conditions for the compressible Navier-Stokes (N-S) equations. In order to validate the developed IB method, direct noise computation is used to simulate the flow-induced noise with both stationary and moving solid boundaries. The paper structure is set up as follows. In **Sec**. 2, the computational models for the flow-induced noise problem are introduced. The body force model based on IMM is derived. Then the high order schemes and the nonlinear nonreflecting boundary conditions (NRBCs) are introduced. In **Sec**. 3, validations for the flow and radiated sound fields from a stationary circular cylinder are conducted to verify the computational models. In **Sec**. 4, the flow field around the harmonically oscillating circular cylinder and the radiated sound field are calculated by utilizing the compressible N-S solver, the influence of oscillating frequency on the vortex shedding and radiated sound are discussed.

2. Computational models for the flow-induced noise simulation

The computational models are established on the fixed Cartesian grid, as shown on Fig. 1(a), to confirm the high-resolution grid for the CAA simulation. The sound generated by the FSI problem is modelled as the cylinder-spring system, as shown on Fig. 1(b).

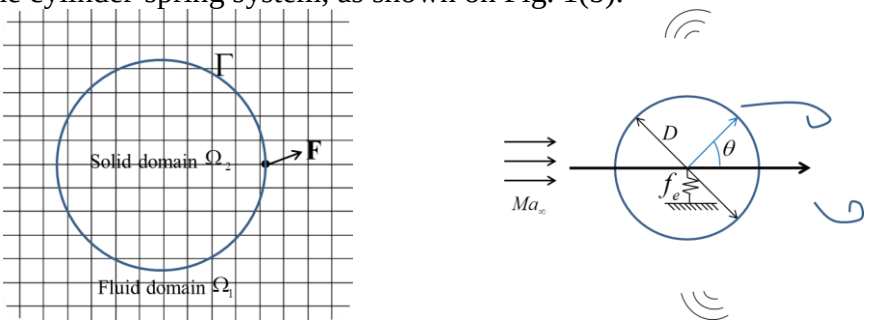

(a) computational domain; (b) schematic model.

Figure 1: Computational domain and the schematic model of the flow-induced noise problem (Γ : the Lagrangian boundary domain; Ω_1 : fluid domain; Ω_2 : solid domain or extended fluid domain; $\mathbf{F}$: the boundary force density; Ma_∞ : inflow Mach number, f_e : the oscillating frequency; D: the characteristic length).

2.1 Governing equations

The flow-induced noise problem can be described by the compressible N-S equations. In computational coordinates, the governing equations (2-D) in conservative form can be written as

$$\mathbf{Q}_t + \mathbf{H}_x + \mathbf{G}_y = \mathbf{S}, \tag{1}$$

where the conservative variables

$$\mathbf{Q} = J \cdot \left[\rho, \rho u, \rho v, E\right]^T, \quad \text{where } E = \rho(u^2 + v^2)/2 + p/(\gamma - 1). \tag{2}$$

and flux vectors

$$\mathbf{H} = J\xi_x \cdot \begin{bmatrix} \rho u \\ \rho u^2 + p - \tau_{xx} \\ \rho uv - \tau_{xy} \\ (E+p)u - u\tau_{xx} - v\tau_{xy} + q_x \end{bmatrix}, \mathbf{G} = J\eta_y \cdot \begin{bmatrix} \rho v \\ \rho uv - \tau_{xy} \\ \rho v^2 + p - \tau_{yy} \\ (E+p)v - u\tau_{xy} - v\tau_{yy} + q_y \end{bmatrix}, \tag{3}$$

with viscous stress terms written as

$$\tau_{xx}=\frac{Ma}{Re}\left[2\mu\frac{\partial u}{\partial x}-\lambda\left(\frac{\partial u}{\partial x}+\frac{\partial v}{\partial y}\right)\right],\ \tau_{yy}=\frac{Ma}{Re}\left[2\mu\frac{\partial v}{\partial y}-\lambda\left(\frac{\partial u}{\partial x}+\frac{\partial v}{\partial y}\right)\right], \tag{4}$$

$$\tau_{xy}=\frac{Ma}{Re}\mu\left(\frac{\partial u}{\partial x}+\frac{\partial v}{\partial y}\right),\ q_x=-\frac{Ma}{(\gamma-1)PrRe}\mu\frac{\partial T}{\partial x},\ q_y=-\frac{Ma}{(\gamma-1)PrRe}\mu\frac{\partial T}{\partial y}, \tag{5}$$

where $\lambda=2\mu/3,\quad \gamma p=\rho T$, and source terms can be written as

$$\mathbf{S}=J\cdot\left[0,\ f_x,\ f_y,0\right]^T, \tag{6}$$

where "^{T}" represents transposition operation, p, ρ, T and u, v denote pressure, density, temperature and flow velocity components in the x and y directions, μ is the viscosity coefficient, which can be calculated by the Surtherland's formula. λ is the second viscosity coefficient. $\mathbf{f}=f_x\mathbf{i}+f_y\mathbf{j}$ is the body force density, $\mathbf{S}$ represents the source term. J is the Jacobian determinant, and ξ_x, η_y are the partial derivatives of the coordinate transformation. Due to the adoption of fixed Cartesian grid, ξ_y and η_x are equal to zero. The length is nondimensionalized by the solid body characteristic length D, velocity by the inflow sound speed c_∞, density by the inflow static density ρ_∞, time t by D/c_∞, pressure by $\rho_\infty c_\infty^2$ and viscosity coefficients by the incoming flow viscosity μ_∞, force by the combined variable $\rho_\infty c_\infty^2 D$. $Ma=U_\infty/c_\infty$ is the Mach number of the incoming flow, and $Re=\rho_\infty U_\infty D/\mu_\infty$, $Pr=0.75$. $\gamma=1.4$.

2.2 IB Method for the wall boundary conditions

In 1972, Peskin [10] firstly constructed the numerical body force model for the FSI problem, based on the Hook's law and generalized function, which is usually classified into the continuous forcing method of IB method. However, it is difficult to model the body force for most of problems especially when the immersed body is rigid. Owing to the simple interpolation operation for the continuous forcing method, Goldstein et al. [6] proposed the feedback forcing method, and Su et al. [11] constructed the relevance matrix of the body force and got a big CFL number. Sun et al. [8] derived the inviscid form of body force for the linearized Euler equations (LEEs). In the following, a more general form of IMM is derived for the compressible Navier-Stokes equations.

The derivation processes can be divided into two steps: prediction and correction steps. In the prediction step, the body force f_x and f_y are set to zero. In physical coordinates, the semi-discretized form of momentum equations can be denoted as

$$\begin{cases}(\rho u)^*=(\rho u)^n+P^n\\(\rho v)^*=(\rho v)^n+Q^n\end{cases}, \tag{7}$$

where P and Q denote the discretization forms of the spatial derivatives for the momentum equations in x and y directions, $(\rho u)^*$ and $(\rho v)^*$ denote temporary conservative variables in the $n+1$ time step. Considering the body force, it is easy to get the exact conservative variables in the $n+1$ time step in the discretized form as

$$\begin{cases}(\rho u)^{n+1}=(\rho u)^n+P^n+f_x\\(\rho v)^{n+1}=(\rho v)^n+Q^n+f_y\end{cases}. \tag{8}$$

Then the body force can be calculated by subtracting Eq. (7) from Eq. (8) as

$$\begin{cases}f_x=\left((\rho u)^{n+1}-(\rho u)^*\right)/\Delta t\\f_y=\left((\rho v)^{n+1}-(\rho v)^*\right)/\Delta t\end{cases}. \tag{9}$$

Based on the coupled equations in Eqs. (10) and (11) also adopted by Peskin [10], the Lagrangian variables and Eulerian variables can be connected by

$$\mathbf{U}(\mathbf{X}) = \int_{\Omega} \mathbf{u}(\mathbf{x})\delta(\mathbf{x}-\mathbf{X})d\mathbf{x}, \tag{10}$$

$$\mathbf{f}(\mathbf{x}) = \int_{\Gamma} \mathbf{F}(\mathbf{X})\delta(\mathbf{x}-\mathbf{X})ds, \tag{11}$$

where $\mathbf{x}=(x,y)$ denotes the Cartesian coordinates, $\mathbf{X}$ is the coordinate vector of the immersed boundaries, $\mathbf{U}=(U_x,U_y)$ is velocity of the immersed boundary points, $\mathbf{F}=(F_x,F_y)$ denotes the Lagrangian boundary force density.

Combining Eqs. (9) (10) with (11), it is easy to get the following equations as

$$\frac{(\rho\mathbf{U})^{n+1}-(\rho\mathbf{U})^{*}}{\Delta t} = \int_{\Gamma_{\mathbf{X}_1}} \left\{ \left[\int_{\Omega} \delta(\mathbf{x}-\mathbf{X}_1)\cdot\delta(\mathbf{x}-\mathbf{X})d\mathbf{x} \right] \cdot \mathbf{F}(\mathbf{X}_1) \right\} ds. \tag{12}$$

Theoretically, the general equations for the boundary force $\mathbf{F}=(F_x,F_y)$ have been obtained without other unknown variables. However, the approximate Dirac delta function in Ref. [10] should be adopted to eliminate the singularity. Then by adopting the Riemann sum in Eq. (12), the discretized form of Eq. (12) can be denoted as

$$\Delta(\rho\mathbf{U})^{T}/\Delta t = \mathbf{A}\cdot\mathbf{F}^{T}, \tag{13}$$

where $\Delta(\rho\mathbf{U})^{T}/\Delta t$ is the momentum variation due to the immersed boundary force. The elements of matrix $\mathbf{A}$ can be expressed as

$$A_{p,q} = \left[\sum_{\mathbf{x}} \delta_d(\mathbf{x}-\mathbf{X}_q)\cdot\delta_d(\mathbf{x}-\mathbf{X}_p)d_x d_y \right] \cdot \Delta s_q, \tag{14}$$

where $p,q=1,M$ (M is the discretized number for the immersed boundaries), δ_d is the approximate Dirac delta function, Δs_q denotes the arc length of the q-th immersed boundaries.

Due to the compact support property for the approximate Dirac delta function, the coefficient matrix $\mathbf{A}$ is highly sparse and can be transformed into positive definite symmetric matrix, therefore two selectable methods can be developed to solve the Eq. (13), one is parallel Cholesky decomposition (PCD) for sparse coefficient matrix, the other is preconditioned conjugate gradient method (PCGM), which can be used to deal with the weakly ill-conditioned matrix.

2.3 Numerical schemes and NRBCs

In the computational model, the seven-points dispersion-relation-preserving (DRP) scheme [12] is adopted to discretize the spatial derivatives of the flux variables in the governing Eq. (1), 2N-storage 5/6-stages low dissipation low dispersion Runge-Kutta (5/6 LDDRK) time marching scheme [13] is adopted to discretize the time derivatives of the conservative variables. In the far-field boundary, the nonlinear perfectly matched layer (PML) absorbing boundary conditions for the Euler equations [14] are adopted. In order to eliminate the spurious short waves near the wall boundary, the selective artificial filter [15] is used, a small filter coefficient 0.03 is found suitable.

3. Results and discussion

In this section, the laminar flows around both the stationary and oscillating 2-D circular cylinder as shown on Fig. 1(b) are simulated. For the simulation parameters, $Ma_\infty = 0.2$, $Re_\infty = 150$ for all the cases, which are same as the stationary case of Inoue et al. [16]. The lift coefficient, drag coefficient and pressure coefficient around the circular cylinder are defined as

$$C_L = F_y/F_0,\ C_d = F_x/F_0,\ C_p = (\overline{p}-p_\infty)/(1/2\rho_\infty U_\infty^2), \tag{15}$$

where $F_0 = 1/2\rho_\infty U_\infty^2 DL$, F_x and F_y are the lift and drag coefficients, and $\overline{p}$ is the time-averaged pressure on the surface of the circular cylinder, $L = 1$ for 2-D problems.

3.1 Validation for the computational model

For the validation experiments, a small computational domain $[-7,11]\times[-7,7]$ is selected to calculate the flow field near the circular cylinder. It's found that even the small computational domain can give a satisfactory result by utilizing the nonlinear PML NRBCs, and the numerical stability can be kept if the CFL number is smaller than 1.2 as shown on Fig. 2, which is excellent among most of the IB method. The grid refinement validations are done for the minimum grid sizes $\Delta x = \Delta y = \pi/180$, $\Delta x = \Delta y = \pi/300$ and $\Delta x = \Delta y = \pi/450$, less than relative 0.5% errors are caused by the grid size $\Delta x = \Delta y = \pi/180$ for the lift and drag coefficients, so in the following simulations, the grid size $\Delta x = \Delta y = \pi/180$ near the solid wall and 0.8 for the CFL number are adopted.

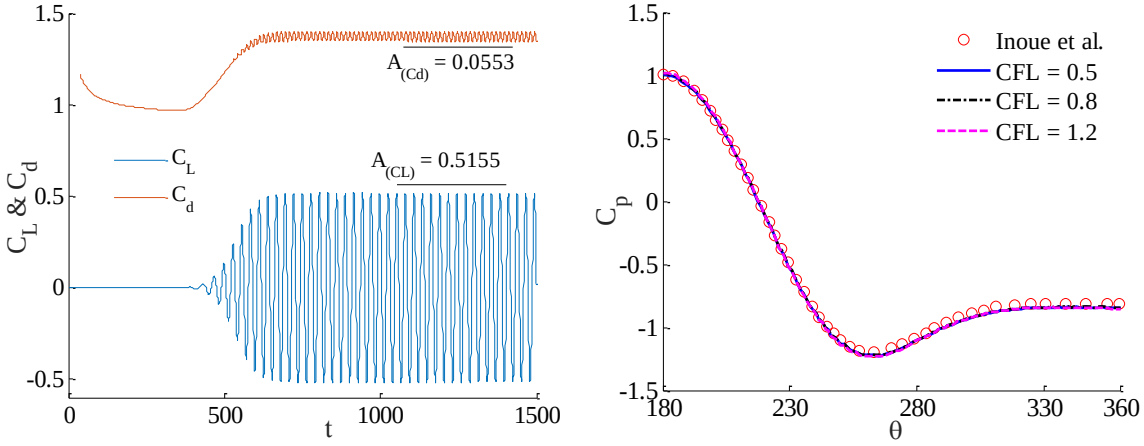

(a) ; (b) .

Figure 2: Instantaneous lift and drag coefficients and pressure coefficient distribution on the surface of the circular cylinder ((a) $\Delta x = \Delta y = \pi/180$, CFL = 0.8; (b) pressure coefficient on the radius $r_p = 0.52$).

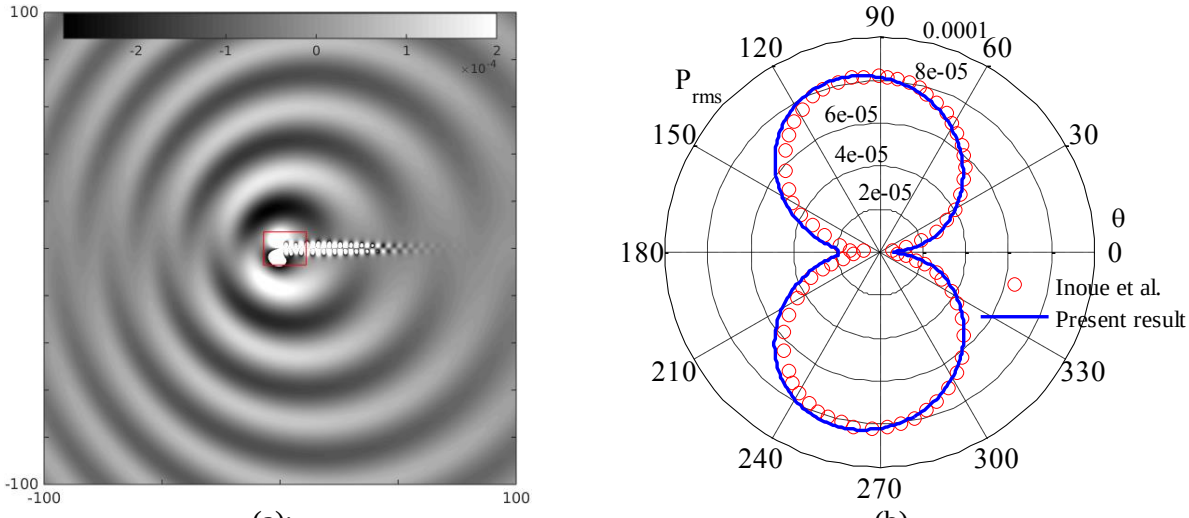

(a); (b).

Figure 3: Comparison for the sound field ((a): instantaneous sound pressure, t=1800; (b): the root mean square of sound pressure on the circle $r_p = 75(1 + Ma_\infty \cos\theta)$).

A large computational domain $[-100,100]\times[-100,100]$ is selected to calculate the radiated sound field, and a stretching factor 1.008 is adopted for the Cartesian grids in *x* and *y* directions. The root mean square of sound pressure is calculated on the circle $r_p = 75(1 + Ma_\infty \cos\theta)$, results are shown on Fig. 3. Good agreements are obtained both for the flow filed near the wall boundaries and the

radiated sound in the far field in the above simulations. It proves that the proposed IB method and computational model are capable of simulating the flow-induced noise problem.

3.2 The radiated sound field for the harmonically oscillating circular cylinder

The oscillating mode of the circular cylinder has a great influence on the vortex shedding and the radiated sound. In this part, the flow and sound fields for a harmonically oscillating circular cylinder are simultaneously simulated. The inflow Ma_∞ and Re_∞ are same as the above. The movement equation for the oscillating circular cylinder is

$$y(t) = A\sin(2\pi f_e t), \tag{16}$$

where A is the oscillating amplitude, f_e is the oscillating frequency. $A = 20\%D$, $f_e = (1.0 \sim 1.2) f_o$ ($f_o = 0.0366$ is the natural vortex shedding frequency for the stationary circular cylinder).

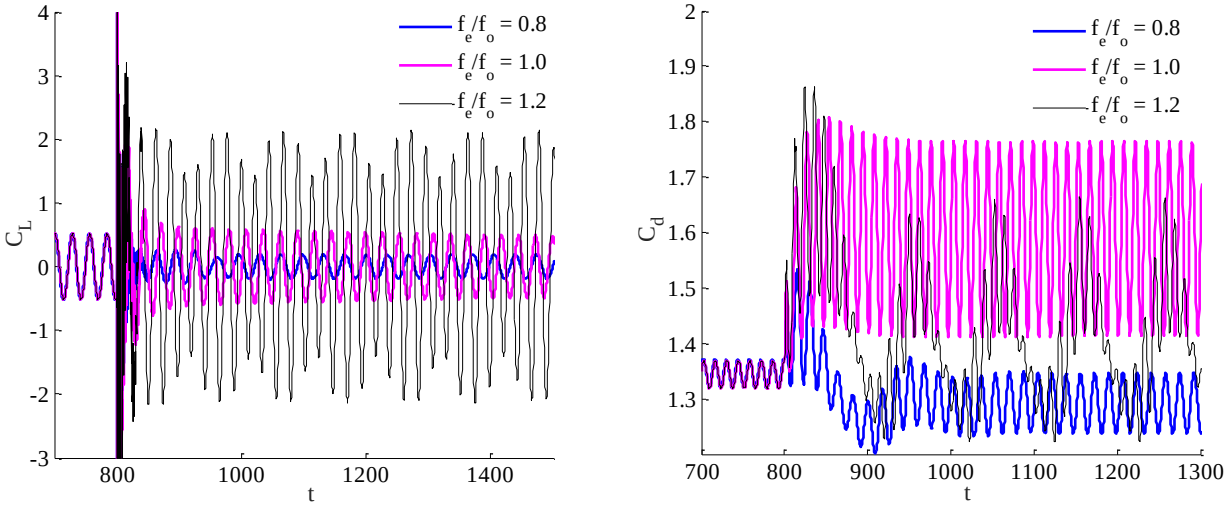

(a) C_L & t; (b) C_d & t.

Figure 4: Instantaneous lift and drag coefficients for different f_e / f_o ratio.

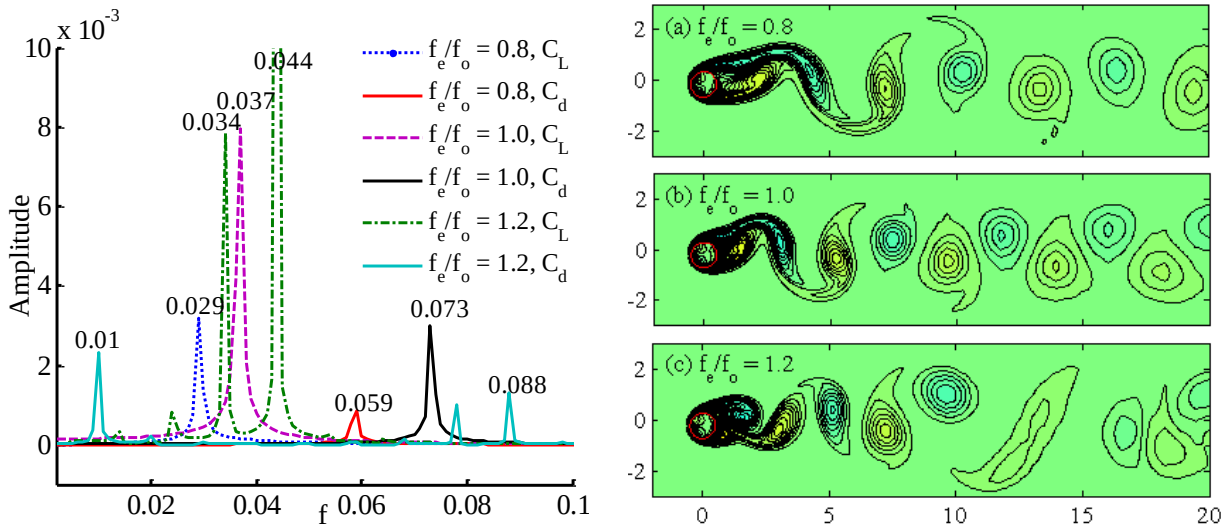

(a) spectrum of the lift and drag coefficients; (b) instantaneous vorticity contours, t = 1500.

Figure 5: The spectrum of the lift and drag coefficients and the flow field near the moving walls.

As shown on Fig. 4 and Fig. 5, the oscillation of the circular cylinder has the tendency to amplify the lift and drag fluctuating amplitudes. The fluctuating amplitudes highly depend on the oscillating frequency ratio. In Fig. 5(a), subharmonic components appears for the lift and drag coefficients,

which means that the vortex shedding presents an obvious nonlinear behaviour as shown on Fig. 5(b).

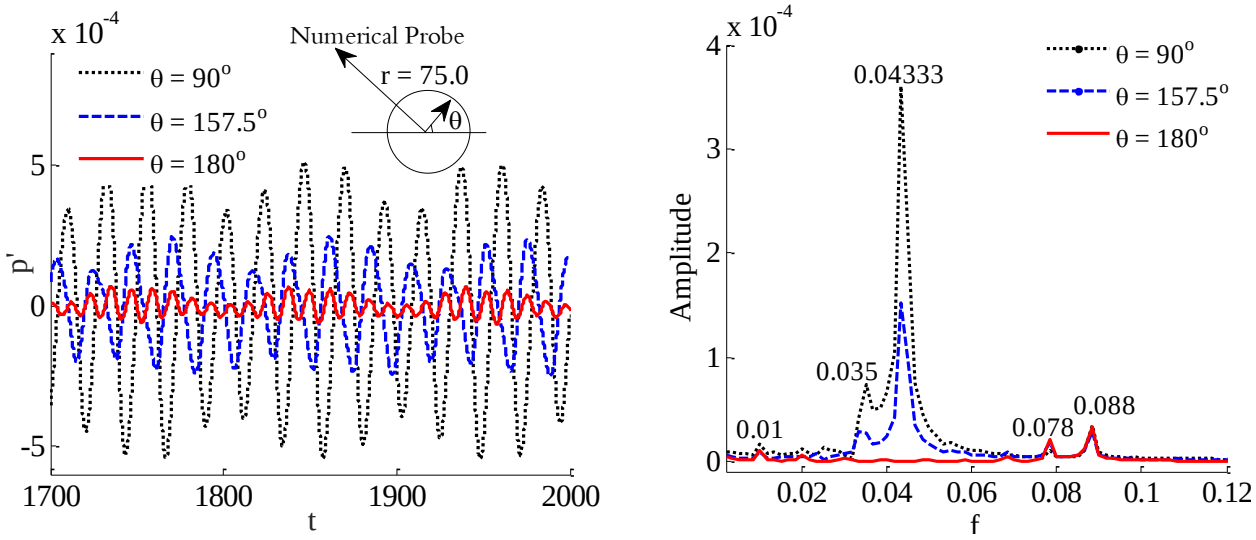

(a) instantaneous sound pressure: $r_p = 75$; (b) frequency spectrum.

Figure 6: The instantaneous sound pressure and the spectrum in the far field ($f_e / f_o = 1.2$).

In Fig. 6(a), the maximum sound pressure fluctuating amplitude appears in the 90° direction. In the 180° direction, an obvious "beat" phenomenon whose frequency is 0.01 appears. And we can see that the drag dipole dominates in the 180° direction, while lift dipole dominates in the others. The sound pressure directivities can be also obtained as Fig. 7.

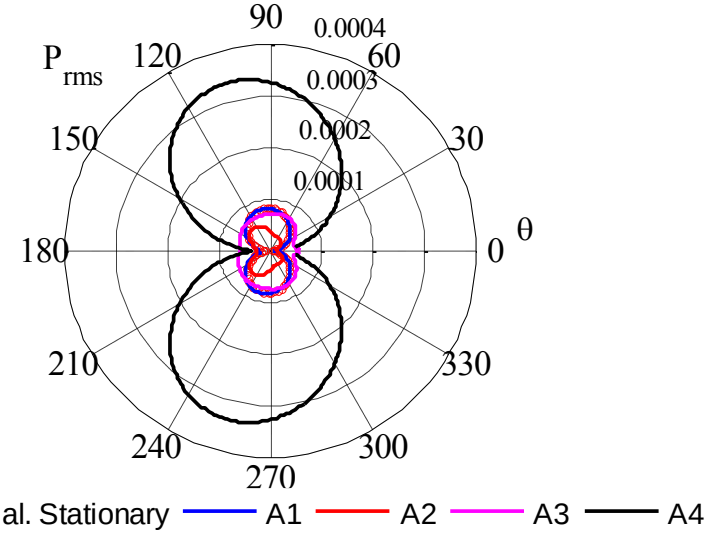

Figure 7: The root mean square of sound pressure on the circle $r_p = 75(1 + Ma_\infty \cos\theta)$ (A1: stationary, A2: $f_e / f_o = 0.8$, A3: $f_e / f_o = 1.0$, A4: $f_e / f_o = 1.2$) .

4. Conclusion

In this paper, a flow-induced noise computational model is proposed. The wall boundary condition is replaced by the constructed body force model. Good agreements are obtained with the previous results both in the flow field near the wall and the sound pressure directivity for the stationary circular cylinder streaming. When the circular cylinder is harmonically oscillating, it's found that the fluctuating amplitudes of the lift and drag coefficients are so greatly influenced that the sound pressure directivities for different f_e / f_o have big differences.

ACKNOWLEDGEMENT

The financial supports from the National Natural Science Foundation of China (Grant No. 11661141020, 51606223) are gratefully acknowledged.

REFERENCES

1 W. Tam, C. K., and Auriault, L. Jet Mixing Noise from Fine-Scale Turbulence, *AIAA Journal*, **37**(2), 145-153, (1999).

2 Dobrzynski, W. Almost 40 Years of Airframe Noise Research: What Did We Achieve?, *AIAA Journal of Aircraft*, **47**(2), 353-367, (2010).

3 Zheng, Z. C., Yang, X., and Zhang, N. Far-Field Acoustics and Near-Field Drag and Lift Fluctuations Induced by Flow over an Oscillating Cylinder, *37th AIAA Fluid Dynamics Conference and Exhibit*, Miami, Florida, USA, 25-28 June, (2007).

4 Nagarajan, S., and Lele, S. K. Sound Generation by Unsteady Airfoil Motions: A Study Using Direct Computation and Acoustic Analogy, *11th AIAA/CEAS Aeroacoustics Conference*, Monterey, California, USA, 23-25 May, (2005).

5 Dowell, E. H., and Hall, K. C. Modeling of fluid-structure interaction, *Annual Review of Fluid Mechanics*, **33**(1), 445-490, (2001).

6 Goldstein, D., Handler, R., and Sirovich, L. Modeling a no-slip flow boundary with an external force field, *Journal of Computational Physics*, **105**(2), 354-366, (1993).

7 Seo, J. H., and Mittal, R. A high-order immersed boundary method for acoustic wave scattering and low-Mach number flow-induced sound in complex geometries, *Journal of computational physics*, **230**(4), 1000-1019, (2011).

8 Sun, X., Jiang, Y., Liang, A., and Jing, X. An immersed boundary computational model for acoustic scattering problems with complex geometries, *The Journal of the Acoustical Society of America*, **132**(5), 3190-3199, (2012).

9 Jiang, Y., Wang, X., Jing, X., and Sun, X. A Study of Three-Dimensional Acoustic Scattering by Arbitrary Distribution Multibodies Using Extended Immersed Boundary Method, ASME *Journal of Vibration & Acoustics*, **136**(3), 1257-1268, (2014).

10 Peskin, C. S. Flow patterns around heart valves: A numerical method, *Journal of computational physics*, **10**(2), 252-271, (1972).

11 Su, S. W., Lai, M. C., and Lin, C. A. An immersed boundary technique for simulating complex flows with rigid boundary, *Computers & fluids*, **36**(2), 313-324, (2007).

12 Tam, C. K., and Webb, J. C. Dispersion-Relation-Preserving Finite Difference Schemes for Computational Acoustics, *Journal of computational physics*, **107**(2), 262-281, (1993).

13 Stanescu, D., and Habashi, W.G. 2N-storage low dissipation dispersion Runge-Kutta schemes for computational acoustics, *Journal of computational physics*, **143**(143), 674-681, (1998).

14 Hu, F. Q., Li, X. D., and Lin, D. K. Absorbing boundary conditions for nonlinear Euler and Navier–Stokes equations based on the perfectly matched layer technique, *Journal of computational physics*, **227**(9), 4398-4424, (2008).

15 Bailly, C., and Bogey, C. Contributions of Computational Aeroacoustics to Jet Noise Research and Prediction, *International Journal of Computational Fluid Dynamics*, **18**(6),481-491, (2004).

16 Inoue, O., and Hatakeyama, N. Sound generation by a two-dimensional circular cylinder in a uniform flow, *Journal of Fluid Mechanics*, **471**(471), 285-314, (2002).